AD-A179 606 LASER CLADDING OF MG AND MO ALLOYS FOR IMPROVED ENVIRONMENTAL RESISTANCE..(U) ILLINOIS UNIV AT URBANA DEPT OF MECHANICAL AND INDUSTRIAL ENG.. 1/1

UNCLASSIFIED J MAZUMDER ET AL. JAN 87 AFOSR-TR-87-0441 F/G 11/6 NL

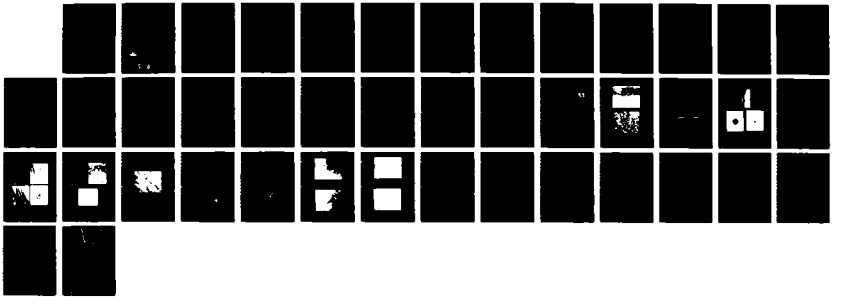

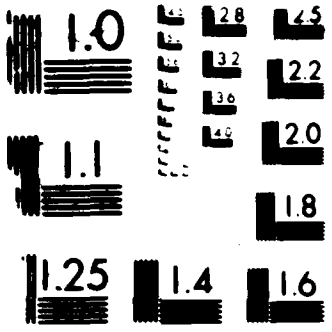
1.0
1.1
1.25
1.4
1.6
1.8
2.0
2.2
2.5
2.8
3.2
3.6
4.0

Annual Report
(January 1986 through January 1987)

LASER CLADDING OF Mg AND Nb ALLOYS FOR IMPROVED ENVIRONMENTAL RESISTANCE

Contract No. AFOSR 86-0034
submitted to
Air Force Office of Scientific Research
Building 410
ATTN: Dr. A. Rosenstein
Bolling Air Force Base
Washington, DC 20332

submitted by

J. MAZUMDER, Principal Investigator,
J. SINGH, Research Associate,
and
S. RAJA, Graduate Research Assistant

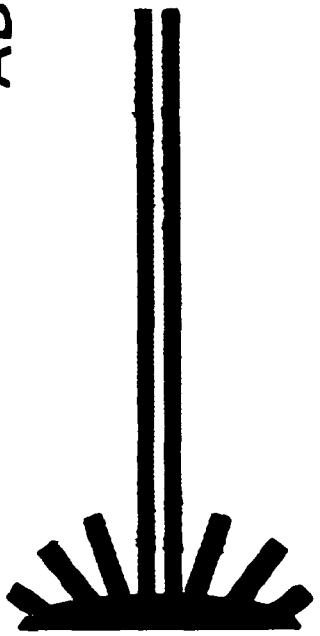

Laser Aided Materials Processing Laboratory
Department of Mechanical and Industrial Engineering
University of Illinois at Urbana-Champaign
Urbana, IL 61801

SECURITY CLASSIFICATION OF THIS PAGE

REPORT DOCUMENTATION PAGE

1a. REPORT SECURITY CLASSIFICATION: Unclassified	1b. RESTRICTIVE MARKINGS
2a. SECURITY CLASSIFICATION AUTHORITY	3. DISTRIBUTION/AVAILABILITY OF REPORT: Approved for public release; distribution unlimited.
2b. DECLASSIFICATION/DOWNGRADING SCHEDULE	
4. PERFORMING ORGANIZATION REPORT NUMBER(S)	5. MONITORING ORGANIZATION REPORT NUMBER(S): AFOSR-TR- 87-0441
6a. NAME OF PERFORMING ORGANIZATION: University of Illinois (6b. OFFICE SYMBOL (If applicable))	7a. NAME OF MONITORING ORGANIZATION: AFOSR
6c. ADDRESS (City, State and ZIP Code): Department of Mechanical & Industrial Engineer, Urbana, Illinois 61801	7b. ADDRESS (City, State and ZIP Code): Bolling AFB, DC 20332-6448
8a. NAME OF FUNDING/SPONSORING ORGANIZATION: Same as 7a (8b. OFFICE SYMBOL (If applicable): NE)	9. PROCUREMENT INSTRUMENT IDENTIFICATION NUMBER: AFOSR-86-0034
8c. ADDRESS (City, State and ZIP Code): Same as 7b	10. SOURCE OF FUNDING NOS: PROGRAM ELEMENT NO: 61102F; PROJECT NO: 2306; TASK NO: A1; WORK UNIT NO:
11. TITLE (Include Security Classification): Laser cladding of Mg & Nb Alloys for Improved Environmen	
12. PERSONAL AUTHOR(S): Dr. Mazumder	
13a. TYPE OF REPORT: Annual	13b. TIME COVERED: FROM Jan 86 TO Jan 87
14. DATE OF REPORT (Yr, Mo, Day):	15. PAGE COUNT: 36
16. SUPPLEMENTARY NOTATION	
17. COSATI CODES: FIELD / GROUP / SUB. GR	18. SUBJECT TERMS (Continue on reverse if necessary and identify by block number):

19. ABSTRACT (Continue on reverse if necessary and identify by block number)

The present status of laser cladding of Mg and Niobium has been surveyed. The potential of cladding Zirconium onto Magnesium and Titanium onto Niobium for improving environmental resistance have been discussed.

In the present project zironium has been cladded onto magnesium by preplaced powder cladding technique. The laser beam encounters the powder first placed on the substrate. A very thin layer on the top of the substrate melts and results in a cladding of minimum dilution.

Corrosion properties of the Zr-clad region was evaluated in a 3.5 percent NaCl solution at room temperature. Substantial improvement in corrosion resistance has been observed. The structural characterization of the clad region was done by optical and electron microscopy. EDAS analysis has been done to identify the phases observed in electron microscopy.

20. DISTRIBUTION/AVAILABILITY OF ABSTRACT: UNCLASSIFIED/UNLIMITED ☐ SAME AS RPT ☐ DTIC USERS ☐	21. ABSTRACT SECURITY CLASSIFICATION
22a. NAME OF RESPONSIBLE INDIVIDUAL: Dr. A. Rosenstein	22b. TELEPHONE NUMBER (Include Area Code): 767-4933 / 22c. OFFICE SYMBOL: NI

DD FORM 1473, 83 APR — EDITION OF 1 JAN 73 IS OBSOLETE

SECURITY CLASSIFICATION OF THIS PAGE

Laser Cladding of Mg and Nb Alloys for Improved Environmental Resistance

S. Raja, J. Singh, and J. Mazumder
Laser Aided Materials Processing Laboratory
Department of Mechanical and Industrial Engineering
University of Illinois at Urbana-Champaign
1206 West Green Street
Urbana, IL 61801

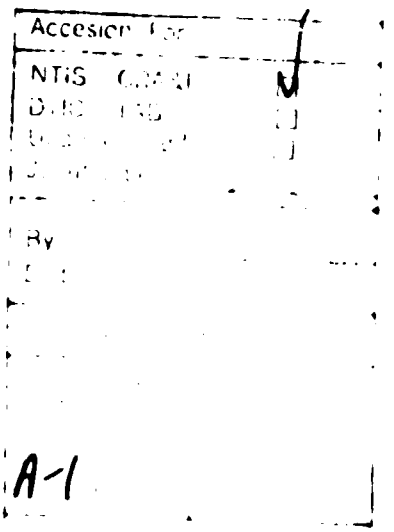

TABLE OF CONTENTS

SUMMARY

The present status of laser cladding of Mg and Niobium has been surveyed. The potential of cladding Zirconium onto Magnesium and Titanium onto Niobium for improving environmental resistance have been discussed.

In the present project zirconium has been cladded onto magnesium by preplaced powder cladding technique. The laser beam encounters the powder first placed on the substrate. A very thin layer on the top of the substrate melts and results in a cladding of minimum dilution.

Corrosion properties of the Zr-clad region was evaluated in a 3.5 percent NaCl solution at room temperature. Substantial improvement in corrosion resistance has been observed. The structural characterization of the clad region was done by optical and electron microscopy. EDAX analysis has been done to identify the phases observed in electron microscopy.

Also titanium has been cladded onto Niobium. DTA thermal analysis of the clad region was done to study the α to β transformation of the Ti-clad region. Variation in the solubility of Nb in Ti clad with laser processing conditions was observed. Corresponding electron microprobe analysis of the Ti-clad region revealed the extent of solubility of Nb in Ti. Structural characterization of the Ti clad region was done by optical microscopy.

The insitu cladding using screw feeder has been proposed and discussed.

I. INTRODUCTION

Much emphasis has been made on laser cladding to modify the surface chemistry of materials to improve properties like wear resistance, corrosion and high temperature oxidation resistance.

Laser cladding is a material processing technique in which a metal or alloy of different composition is deposited onto the substrate. The substrate is locally melted by using laser beam to produce metallurgical bonding. The metal deposited onto the substrate and only thin layer of the top surface of the substrate are melted by the laser beam on account of high power density available from the focused laser beam. The localized heat source of laser with low specific energy input in conjunction with very short laser-material interaction time keep the substrate at low temperature and make the substrate as an intimate heat sink. The novel microstructure results from the high cooling rate. The best cladding is considered to be the one with minimum dilution of the clad layer on the substrate with a thin layer of interface between them.

The processing variables that influence the laser surface cladding are: power of the laser beam, beam diameter, spatial distribution, traverse speed, the chemistry of the substrate, and focusing conditions [1].

Under controlled cladding conditions, a laser beam melts a very thin surface layer of the substrate. This thin liquid layer mixes with the liquid cladding alloy and subsequently solidifies to form a metallic bonding between the cladding and substrate. A scheme has to be developed to choose the best combination of the processing variables for a particular application.

From the literature, it has been found out that laser surface alloying and laser cladding have been done by using either of the following methods to deposit the metal onto the substrate.

1) sputter-deposition [2]

2) electro deposition of thin film [3]

3) spraying or coating the metallic powder [4]

4) gas-borne injection of powder into the laser interaction zone [5].

Selective improvement of properties by material processing and subsequent microstructural studies have been done by using different techniques [6,7,8,9] such as rapid solidification process (RSP), laser alloying, plasma spraying and electron beam rapid quenching (EBRQ) process. The final microstructure obtained by this technique depends mainly upon heat and mass transfer, fluid flow and cooling rate.

Studies have been done on the microstructure and corrosion properties of laser irradiated Mg-Zn alloy [10]. In laser beads deposited on Mg-5.3% Zn-0.6% Zr alloy the microstructure was finely dendritic. Due to high cooling and growth rates the material was very homogeneous. Corrosion studies have revealed that corrosion rate of rapidly solidified Mg-Zn alloy immersed in a 3.5% NaCl aqueous solution is higher than that in a slowly solidified specimen. This increase in corrosion resistance has been attributed to the formation of finely distributed interdendritic nonequilibrium Mg_7Zn_3 phase.

Irradiation with a CO_2 laser at 40 w/mm^2 refined the microstructure of the Mg-Li alloy to a depth of 1.5 mm and raised its corrosion resistance [11]. In the laser affected zone, the alloy has a homogeneous fine-grained microstructure with an average grain size up to 2 μm. The corrosion resistance of this Mg-Li alloy in a 3% NaCl solution was shown to increase by a factor of 30 after irradiating the surface by a pulsed laser and by more than an order of magnitude following irradiation by a continuous wave laser. The increase in corrosion resistance has been attributed to the grain refinement and absence of structural defects.

The main aim of the present investigation is to study: (1) the corrosion properties of cladding of Zr onto the Mg substrate, and (2) high temperature oxidation resistance of laser clad Nb alloys. To the best of the authors' knowledge, the corrosion studies of laser clad Mg-Zr system and Nb alloys have not been reported in the literature.

It is reported that the structural refinement, achievemert of non-equilibrium phases and extremely homogeneous amorphous alloys concomitant of very high cooling rate prevailing under laser processing conditions improve the oxidation and corrosion properties considerably. The rationale for choosing Zr as the cladding metal for Nb is to generate these phases which are proven resistant to corrosion and oxidation in several alloy systems such as Nb-Ti-Zr [12], Nb-Zr [13], Nb-Mo-Zr [14], and Nb-Ti-Al-Zr [15].

Studies of laser-alloyed zirconium-containing surface layers have been reported [16]. Thin films of Zr on Fe, Ni, Al, V, and Ti have been alloyed with the substrate metals using the pulse laser.

The recent review [17] of the current state of the art of coating systems classifies the coatings available under two headings: "metallic coatings" and "ceramic thermal barrier coatings". Among the coating techniques laser cladding has unique potentials: production of extremely homogeneous amorphous alloy phases on account of rapid cooling rate prevailing under laser-material processing conditions, less loss of materials, feasibility of controlling alloy chemistry, minimized dilutions, minimized distortion and minimized post processing machining [18].

Laser cladding of Nb with Ti is carried out in this experiment. In the literature there are no reports dealing with the oxidation behavior of laser cladded Nb alloys. A sizeable body of the literature deals with high temperature oxidation properties of surface coated Nb-alloys. In these cases

surface coating has been done by diffusion using liquid metal as transport medium. The diffusion coating has been subsequently oxidized to produce transient oxide layer which is found to improve the oxidation resistance. In the diffusion coating of Nb, liquid Na was used as transport medium [2] since it is immune to corrosion in this medium. The kinetics of diffusion coating is very slow and almost 10 to 12 hours dipping has to be done at temperatures as high as 1200 to 1300°C. This coating was followed by rapid cooling to develop finer microstructure which results in improved oxidation resistance.

Some of the Nb alloys which have been studied and experimented with heat resistant coatings are given below; it is important to note that in all these cases, the coating has been done by diffusion in liquid metal medium.

1. Nb - 1 at % Zr [19]
2. Nb - 10, 20, 30 wt%, Ti [20]
3. Nb - Al [21]
4. Nb - 5W - 3 Mo - 1 Zr - 0.02 C [22]
5. Nb - 5% Mo - 1% Zr [23]
6. Nb - 40% Ti - 3-7% Al, 0.06% C [24]

It has been reported that the Nb-alloy substrates given above have been alloyed or coated with either of the following alloying elements.

1. Al, Zr, Cr, Mo [25]
2. Mo-B-Si [26]
3. Si-Ti [22]
4. Cr-Si-Ti, Mo [27]
5. Zr, V [28]
6. Ti, Ta [29]
7. Cr, V [30]

8. Re, V, Pt, Si, Cr [31]

9. Ti, Al [32]

Perrin [20] has studied the influence of Ti content on oxidation of Nb-Ti alloys. Ti is found to form protective oxide layer and oxygen diffusion is the preponderant mechanism of oxidation. Ti has been increased in Nb from 10 to 30 wt% and oxidation test has been carried out in air at 400 to 1300°C. Depth of oxygen penetration decreased with increase in Ti content. Above 700°C, Ti addition in Nb gave parabolic oxidation rate which implies the protective nature of oxide scale.

Pure Nb has poor oxidation resistance [33] above 300°C and appreciable high temperature strength (Table 3). But the alloys with Ti, as in the case of pure Ti, hardly oxidize at all up to 800°C. There has been a considerable decrease in the constant of parabolic oxidation rate at 1000°C. Also there was a change in the type of oxidation rate at 1200°C, it changed from linear to parabolic. Introduction of Ti into Nb caused a considerable improvement in the scale resistance which increased with increasing Ti content.

The oxidation of Nb base alloys has been studied by several authors [34-37] and among these alloys, the Nb-Ti alloys exhibit improved oxidation resistance [20]. In this regard, another aim of the present investigation is laser cladding of Ti onto Nb substrate and evaluation of oxidation properties of the clad.

II. EXPERIMENTAL PROCEDURE

The experimental set-up for laser cladding is shown in Fig. 1. It consists of a stainless steel chamber. Ar gas was used to maintain an inert atmosphere inside the chamber at a pressure 20 psi inside the chamber. It provided shielding of the substrate which minimized the surface contamination and prevent oxidation of Mg which is pyrophoric. The plasma formation at the laser-substrate interaction point was also suppressed by the Ar atmosphere and above atmospheric pressure.

The cladding treatments were carried out using a continuous wave CO_2 laser with 1.5 kW. In the present investigation, laser was operated at 800-1000 W in the TEM^*_{00} mode (Gaussian distribution). The cladding was performed with an underfocused beam of 1.5 to 3 mm diameter. Mg specimens (63.5 mm thick) were traversed relative to the laser beam at the speed of 20 to 50 inches per minute.

Zr powder used was 99.99% pure with particle size 20 μm supplied by Johnson Matthey, AESAR. Zr powder was directly applied on to the Mg specimen and compacted to prevent loose packing.

The formation of cracks due to thermal shock by rapid heating and cooling rates during laser processing was prevented by preheating the Mg substrate by laser interaction.

Ti has been cladded onto Nb using a 10 kW CW CO_2 laser. Prior to cladding the Ti powder (99.9 percent pure, supplied by Johnson Matthey, AESAR) was annealed in a temperature controlled tubular furnace for about 16 hours to get rid of moisture. The cladding was carried out by placing the powder on the Nb cylindrical specimen (20 mm height, 12.57 mm dia.) prior to laser-metal interaction.

The laser cladding process variables used are in the following range:

Laser power: 4 to 8 kW

Laser beam diameter: 3 mm

Scanning speed: 20 to 50 ipm (inches per minute)

For the optical microscope observation, an etchant of 3% HNO_3 in methanol was used for Mg-Zr clad, and an etchant of 5 ml HNO_3, 2.5 ml HF and 17.5 ml water was used for Nb-Ti clad. The optical microscope used was LEITZ.

Microstructural investigations of clad specimens were carried out by optical and Electron Microprobe Analysis (EPMA) and electron microscopy. Samples for transmission electron microscopy were sectioned in the laser clad region. After mechanically thinning the samples, discs of 3 mm diameter were punched from the clad region. Specimens for TEM observations were prepared by dimpling followed by ion-beam thinning technique by using Ar ion-beam at an angle of 12° to the surface in a cold chamber to avoid phase transformation of metastable phases due to heat developed during ion bombardment. The TEM samples were observed using philips EM 430 microscope (attached with EDAX), operated at 300 kV.

The corrosion studies of Mg alloys were carried out in EG&G PARK corrosion testing system (Fig. 2). Sections from the clad region parallel to the clad/substrate interface were cut and exposed to 3.5% NaCl solution. Potentio dynamic and corrosion potential testings were carried out at room temperature.

The differential thermal analysis (DTA) of the Nb-Ti clad region was carried out using Perkin-Elmer 1700 Differential Thermal analyzer. The sampling for DTA was done as follows: thin sections of the clad region were cut normal to the clad/substrate interface using Buehler ISOMET low speed diamond saw. The samples were subsequently cleaned using acetone and dichloroethane.

The thermal analysis was carried out with the following experimental variables:

T_{min} : 100°C

T_{max} : 1500°C

Heating Rate 40°C/min

Cooling Rate 40°C/min.

Ar was used for the cooling curve determination at the flow rate of 30 cc/min.

III. RESULTS AND DISCUSSION

3.1 Magnesium-Zirconium Alloy

3.1.1 Optical Microscopy

The general microstructural survey of the laser clad region by optical microscopy revealed two distinct phases (Fig. 3a and 3b).

The clad region is divided into two parts (Fig. 3a): the lower zone shows duplex microstructure of two phases and the upper zone shows homogeneous microstructure. The electron microprobe analysis of laser clad/substrate region is shown in Fig. 4. The width of the lower zone, which is adjacent to the clad/substrate interface, is approximately 200 μm.

The optical micrograph near the interface at a higher magnification (Fig. 3b) shows the two phases. The microprobe analysis in the bottom zone shows the depletion of Mg at a point where Zr is enriched and vice versa. This suggests two phases one rich in Mg and another rich in Zr exist near the interface. By contrast and the microanalysis, the bright phase was found to be rich in Zr.

3.1.2 Electron Microscopy

The general microstructural survey of the laser clad region by transmission electron microscopy (TEM) revealed several phases: amorphous, crystalline, precipitates, and matrix with high density of dislocations.

3.1.2.a Amorphous Phase

In a thin foil prepared from the clad region it was observed in the TEM that an amorphous region was contiguous to a crystalline region. This is shown in the bright field (BF) micrograph in Fig. 5a. Figure 5b shows

the selected area diffraction pattern (SAD) from the region marked 'A' in Fig. 5a and the diffused rings shows that region 'A' is amorphous. Figure 5c shows the SAD pattern from regions marked 'B' and 'C' and consist of diffuse rings due to amorphous phase and diffraction spots due to crystalline phase in these regions.

The X-ray microanalysis of the amorphous phase is shown in Fig. 6. The quantitative microanalysis from amorphous phase (region A) revealed that this phase contains 85.56 wt% Zr and 14.439 wt% Mg.

The X-ray microanalysis of the region B is shown in Fig. 7. The quantitative analysis done for the EDAX spectrum from this region revealed that this region contains equal amount of Zr (50.56 wt%) and Mg (49.431 wt%).

The X-ray microanalysis of the region marked C is shown in Fig. 8. The quantitative analysis done for the EDAX spectrum from this region revealed that this region is rich in Mg (74.464 wt%) and depleted in Zr (25.536 wt%).

From the electron microscopic investigation in conjunction with X-ray microanalysis, an amorphous phase rich in Zr and an interface containing equal amount of Zr and Mg and an adjacent region rich in Mg were found. The amount of Mg increases as one move from the amorphous phase towards the interface.

Similar findings have also been observed in Cu-Zr system [38]. Amorphous surface layer 30 to 70 μm thick in the alloy Cu-43 at % Zr by laser radiation under suitable condition has been reported in the literature. It is reported that, even on melting treatment at larger areas by overlapping pulse irradiation, the glassy structure may be retained in the topmost structure.

Capelli [39] has pointed out the attainment of amorphous alloys by laser glazing. The extremely rapid cooling rates of thin molten zones formed by laser interaction have produced a variety of novel, extremely homogeneous microstructure, including amorphous alloys.

3.1.2.b Martensite Phase

As mentioned above, in the clad region, martensitic phase has been found in TEM study. The bright field micrograph of martensitic phase is shown in Fig. 9a.

The dark field micrograph formed by one of the Bragg reflections from the martensitic phase is shown in Fig. 9b. This shows lath type martensites. The dark field image formed by one of the matrix reflections is shown in Fig. 9c. This shows heavily dislocated matrix.

The diffraction pattern in Fig. 9d shows the diffraction spots from the matrix as well as martensite. The streaking effect along one direction is observed.

3.1.2.c Precipitates

Figure 10a shows the bright field image of precipitates and strain contrast due to the shear imposed by the precipitates. The dark field image of the precipitate formed by one of the reflections from the precipitate is shown in Fig. 10b. The average size of the precipitate was found to be 0.02 μm and found to be uniformly distributed. Figure 10c shows the diffraction pattern, from the precipitate region.

3.1.3 Corrosion Properties of Laser Cladding of Zr onto Mg

The corrosion properties of the laser clad and pure Mg have been evaluated.

Figure 11a shows the optical micrograph of laser clad region. The microstructure reveals the Zr rich phase and Mg rich phase.

The results from corrosion potential test and potentio dynamic test have been shown in Figs. 12a and 12b, respectively for pure Mg and in Figs. 13a and 13b, respectively for clad region.

The results from these corrosion studies have been summarized and compared with other metal and alloy systems in Table 2.

The formation of homogeneous amorphous phase enriched in Zirconium is manifested in increase in the corrosion potential.

3.2 Niobium-Titanium Alloy

The α to β transformation of Ti has been studied by using differential thermal analysis, optical microscopy and electronprobe microanalysis. The optical micrographs in Figs. 14 and 15 show the widmanstätten structure of α and β transformation of the Ti clad for the parameters, 8 kW and 20 ipm. Figures 16 and 17 show the optical micrograph of Ti clad for the parameters, 6 kW and 20 ipm.

The DTA-heating curve of Ti clad region (6 KW, 20 ipm) is shown in Fig. 18. There is no appreciable shift in the α to β transformation temperature of the clad from that of pure Ti. The transformation occur around 860°C. The corresponding EPMA-analysis of this clad region is shown in Fig. 19 and the amount of Nb dissolved in the Ti clad near the interface is found to be seven weight percent.

The DTA-heating curve of Ti clad region (8 kW, 20 ipm) is shown in Fig. 20. The appreciable shift in the α to β transformation temperature towards lower temperature range suggests the increase in the amount of Nb in the Ti clad region. The corresponding EPMA analysis of this clad, as shown in Fig. 21, shows the increase in the amount of Nb dissolved in the clad to 10 weight percent.

According to the equilibrium phase diagram of Nb-Ti system, as shown in Fig. 22, the increased amount of Nb in the Ti clad region is due to extended solid solubility. Transmission electron microscopy has to be done to analyze the phases present in the clad.

IV. FUTURE WORK

The method employed to deposit the metal onto the substrate and the type of laser-metal interaction affect the extent of mixing (mass transport) and the resultant cooling rate (heat transport). This in turn influence the overall composition and microstructure of the laser clad material. On account of rapid solidification conditions prevailing in the laser cladding technique, usually fine microstructure, increased solid solubilities of alloying elements, nonequilibrium crystalline and amorphous phases and achievement of high point defects have been observed and reported widely in the literature.

The cladding of Zr onto Nb by insitu cladding technique has been proposed. A screw feeder to deliver the zr powder into the laser zone has been developed (Fig. 23). The laser beam encounters both the substrate and the powder delivered from the screw feeder simultaneously. The result is change in heat and mass transfer conditions from normal cladding technique by preplacing the powder onto the substrate before laser metal interaction. The change in microstructure and the corrosion resistant properties have to be studied.

The addition of Zr improves the oxidation properties of Nb alloys by forming ZrO_2 particles dispersed in the matrix. In case of an alloy Nb-1% Zr prepared in the ingot metallurgy route, low temperature saturation of the alloy with oxygen favors the formation of ZrO_2 particles. This work emphasizes the increased diffusion mobility of Zr atoms in Nb at 900°C.

It has been observed, in the Nb-Zr alloy, that Zr on rapid cooling gives rise to martensitic type of transformations [12].

In this regard, laser cladding of Zr onto Nb using insitu powder feeding technique has been proposed. A screw feeder has been designed to deliver the metallic powder into the laser interaction zone on the substrate directly.

This insitu cladding technique affects the mass and heat transfer and the formation of metastable phases.

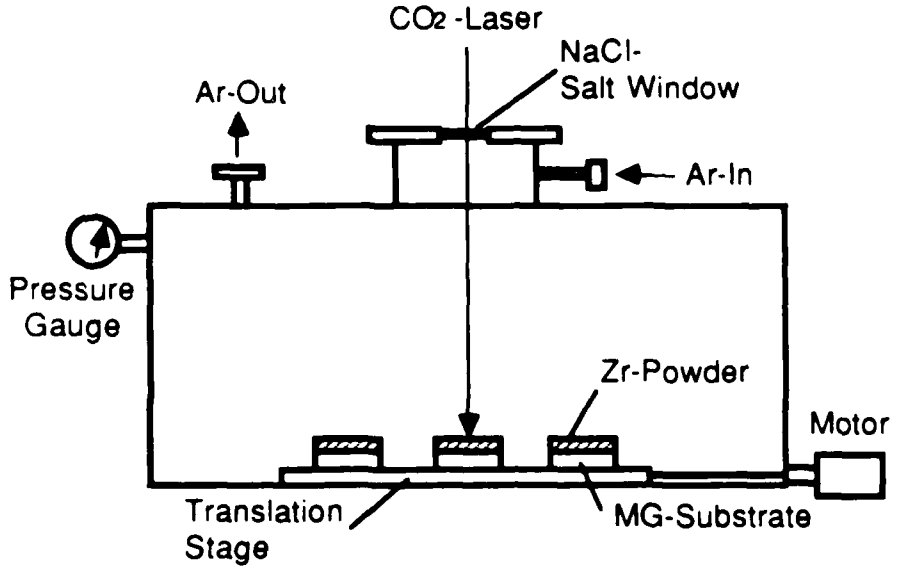

Fig. 1 Experimental Setup for Cladding

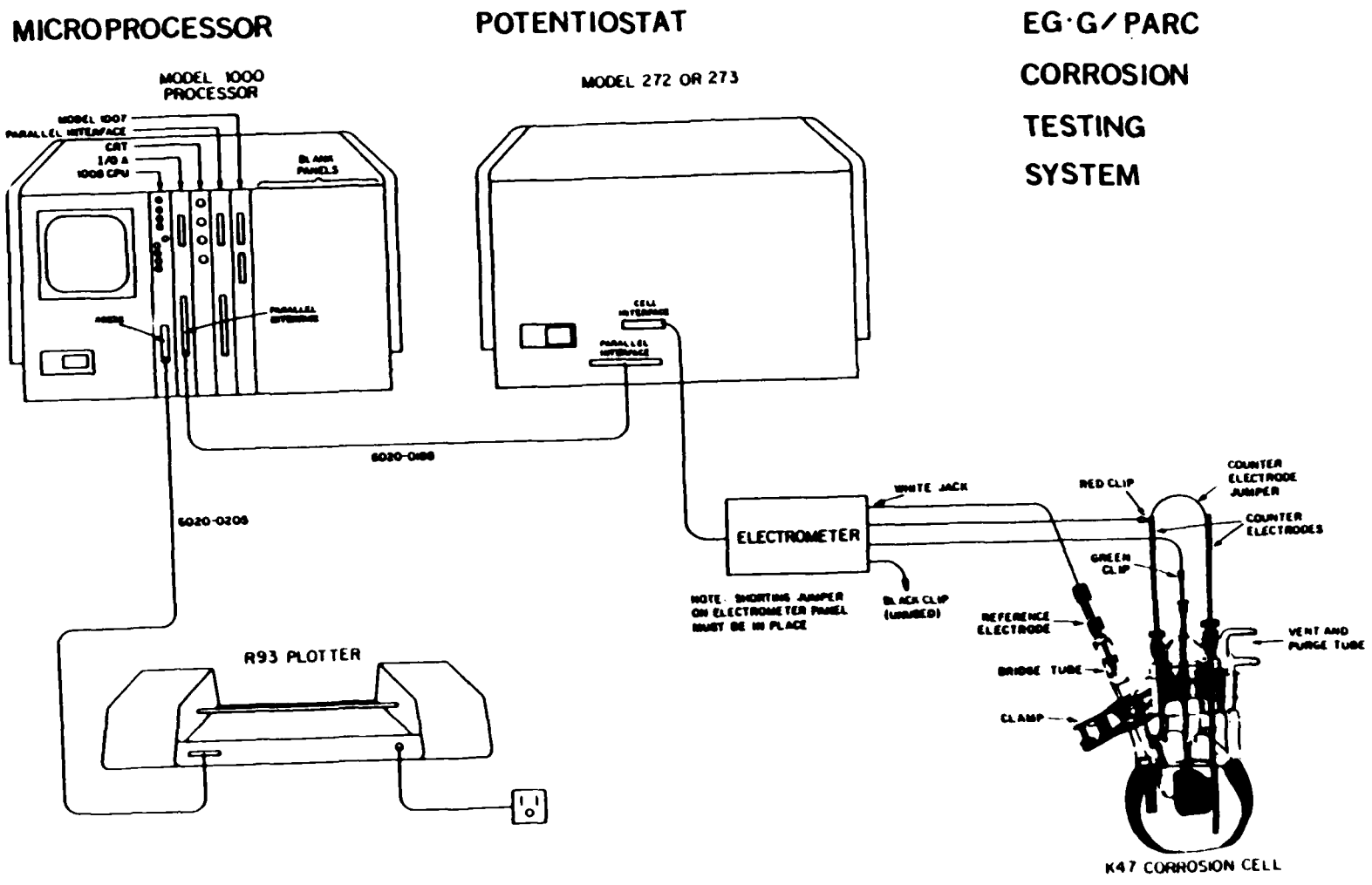

Fig. 2 EG.G/Park Corrosion Testing System

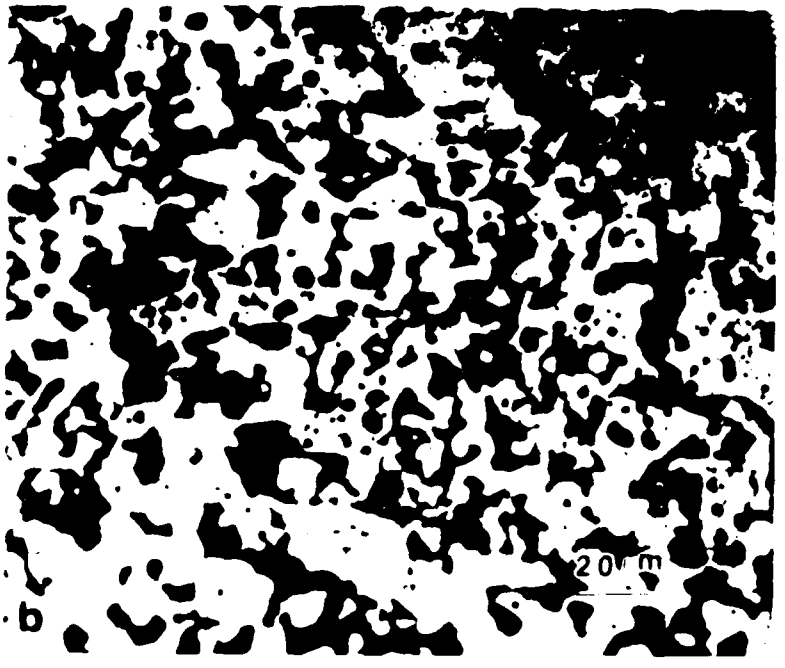

Fig. 3a and b Optical Micrographs of Ir on Mo Clad Region

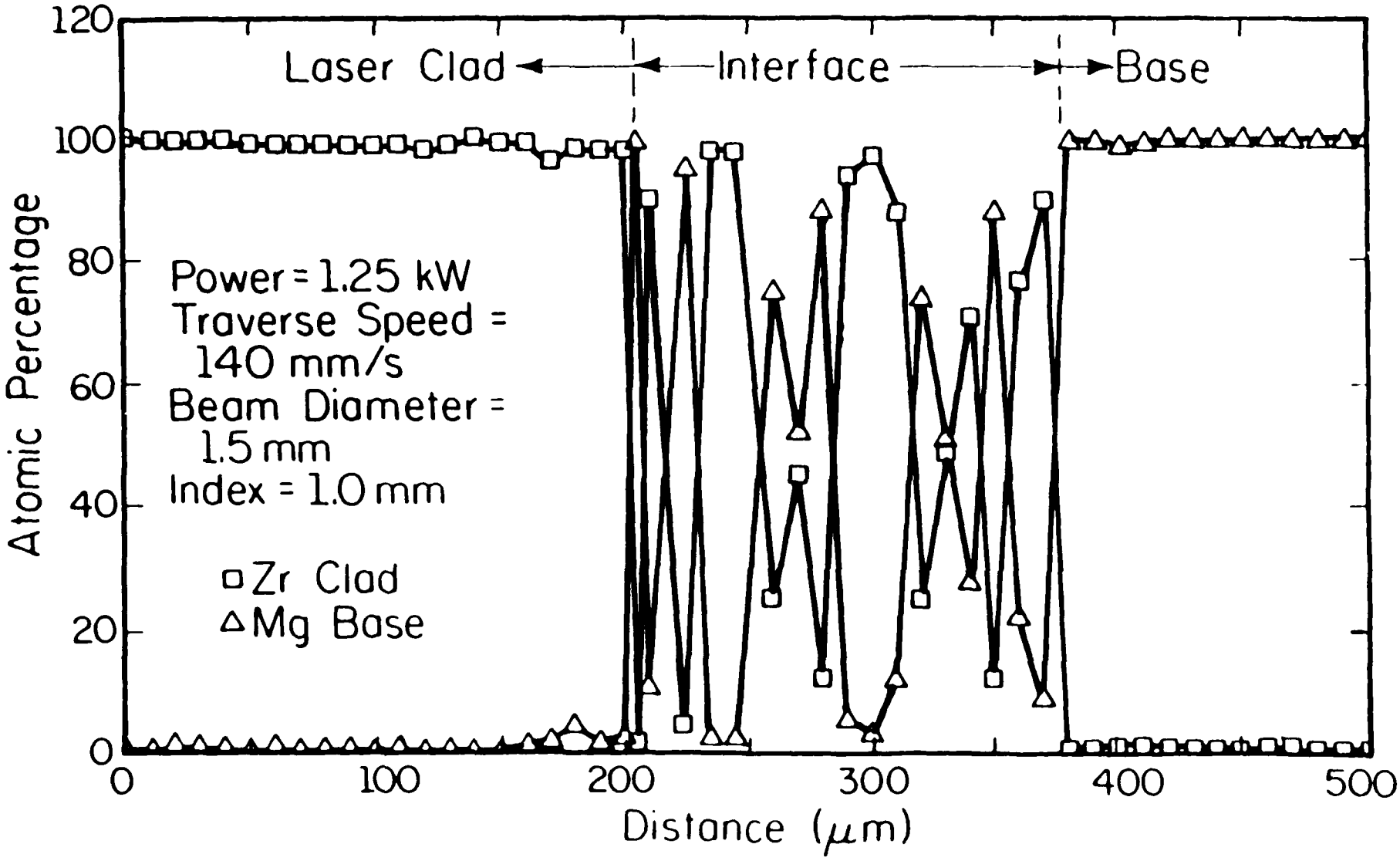

Fig. 4 EPMA (Electron Probe Mirco Analysis) of Clad/Interface/Substrate

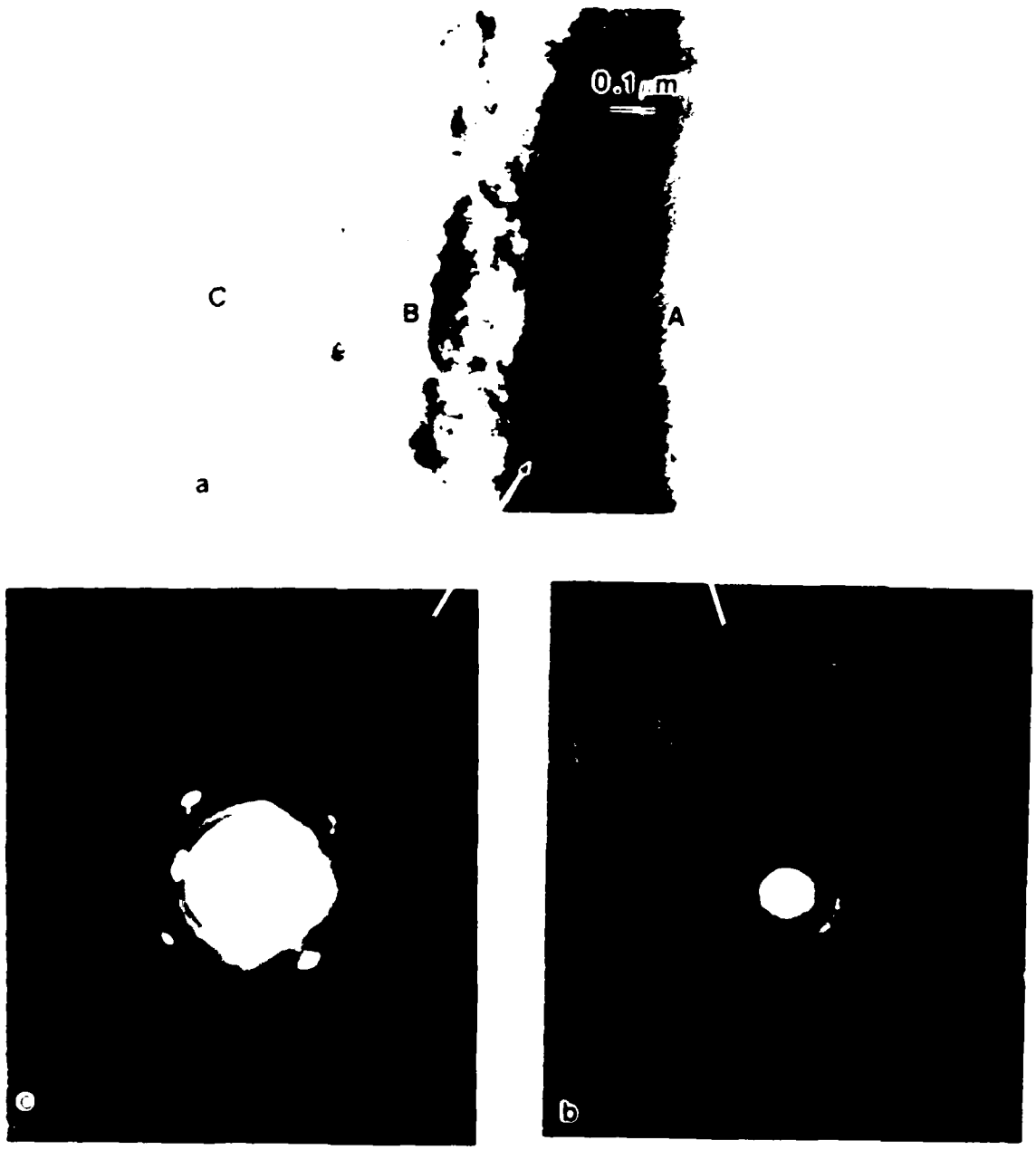

Fig. 5a Electron Micrograph of Clad Region

b Selected Area Diffraction (SAD) Pattern from Amorphous Region

c SAD Pattern from Crystalline Amorphous Interface

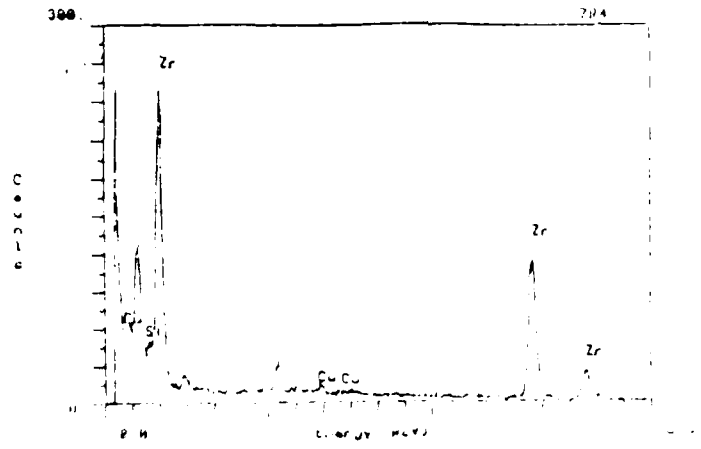

Fig. 6 EDAX (Energy Dispersive Analysis by X-ray) Spectrum from Amorphous Region

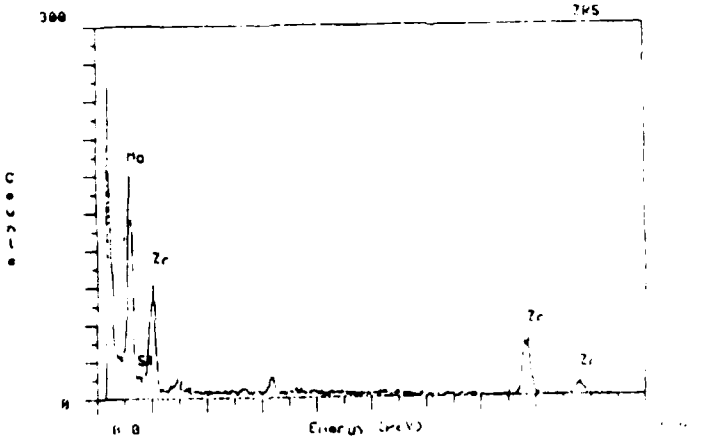

Fig. 7 EDAX Spectrum from Crystalline Amorphous Interface Region

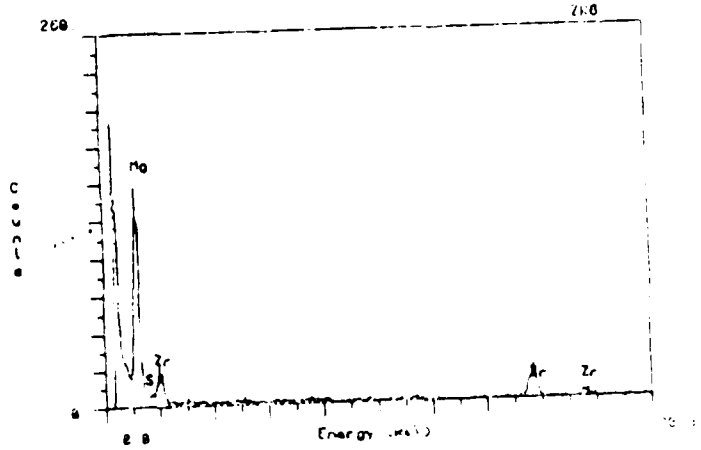

Fig. 8 EDAX Spectrum from a Region Adjacent to Crystalline-Amorphous Interface

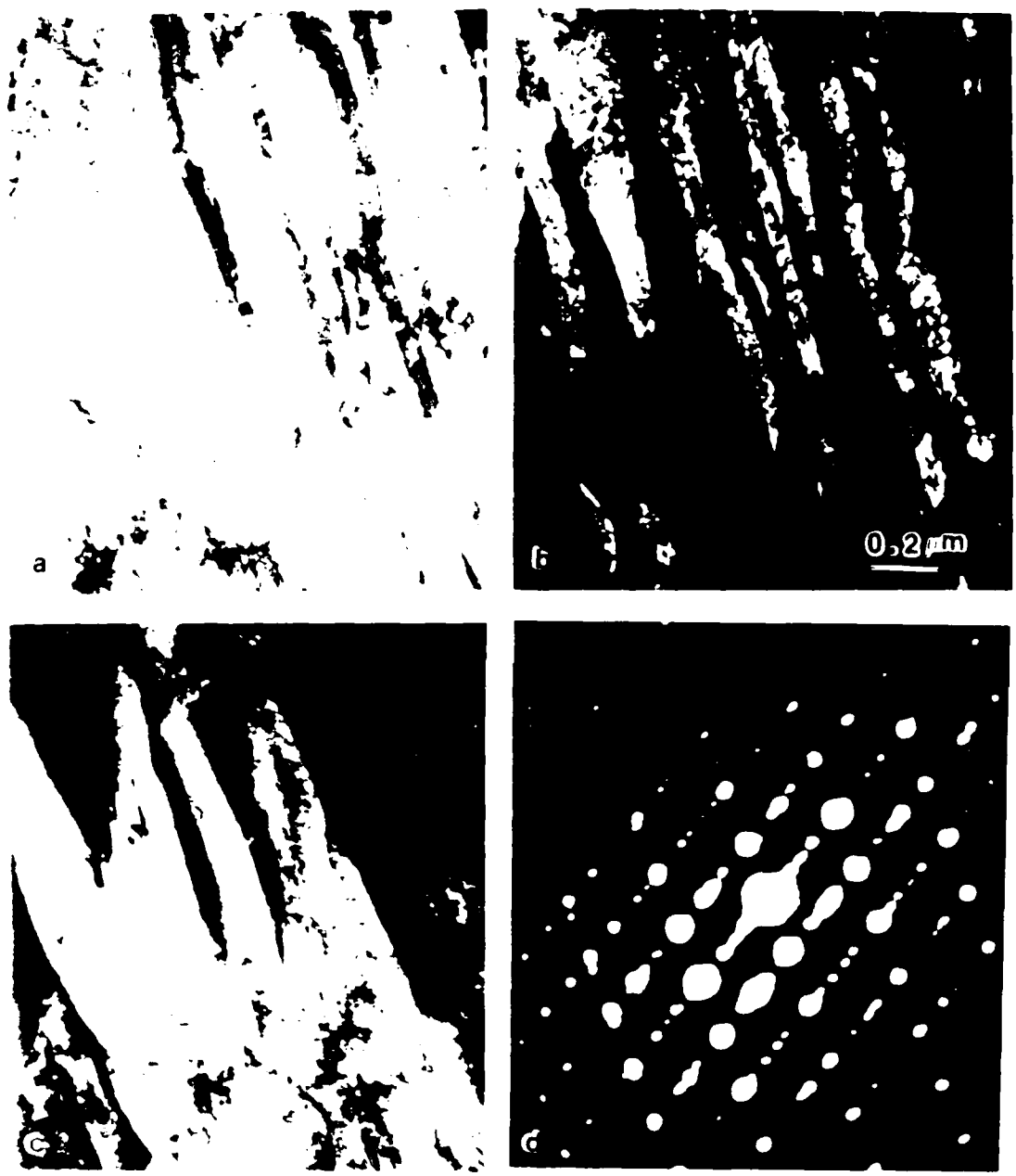

Fig. 9a Bright Field (BF) Electron Micrograph of Martensitic Phase

9b Dark Field (DF) Electron Micrograph formed by one of the Reflections from Martensitic Phase

9c DF Electron Micrograph Formed by one of the Matrix Reflections

9d Diffraction Pattern from Matrix and Martensite Phase

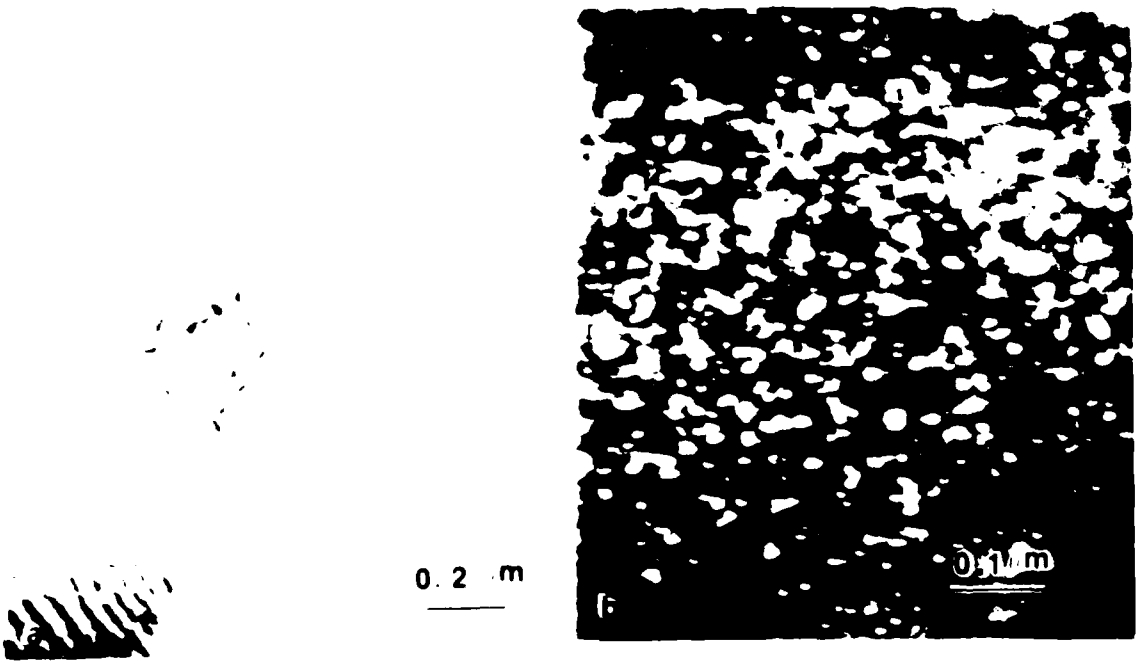

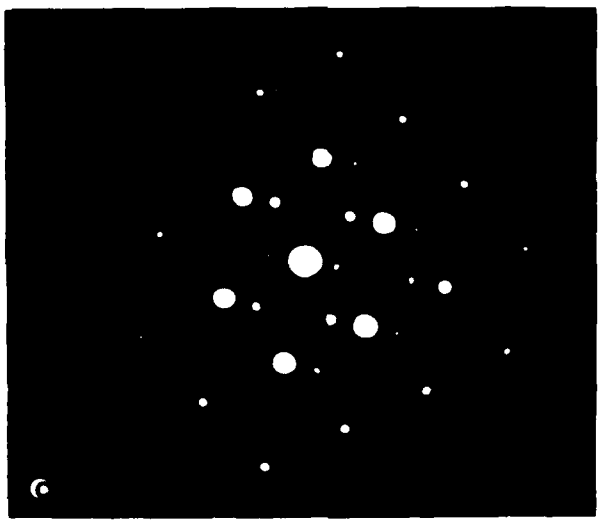

Fig. 10a BF Electron Micrograph of Precipitate Region

10b BF Electron Micrograph of Precipitate Region

10c Diffraction Pattern from Precipitate Region

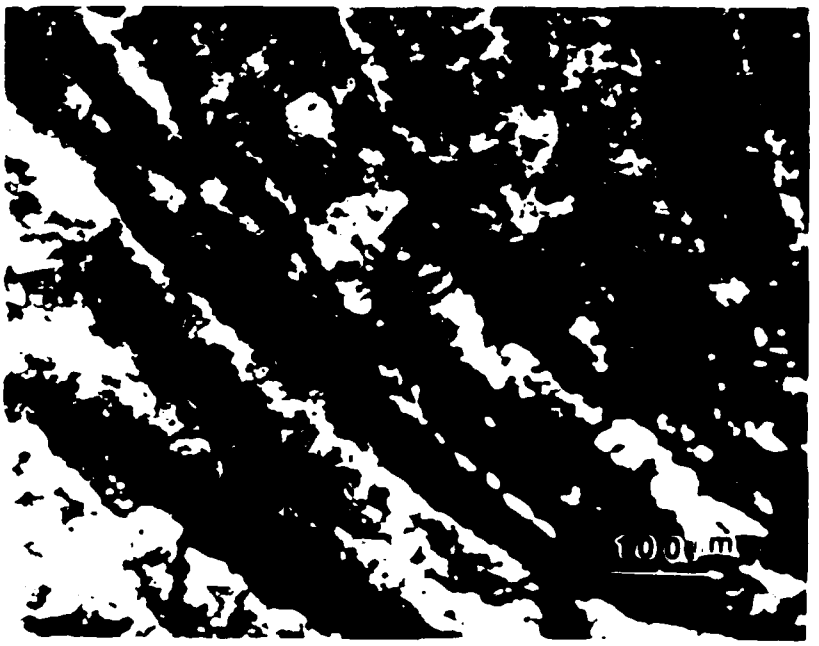

Fig. 11 Optical Micrograph of Zr Laser Cladded onto Mg - The Clad Region

Fig. 12a corrosion Potential Plot of Pure Mg

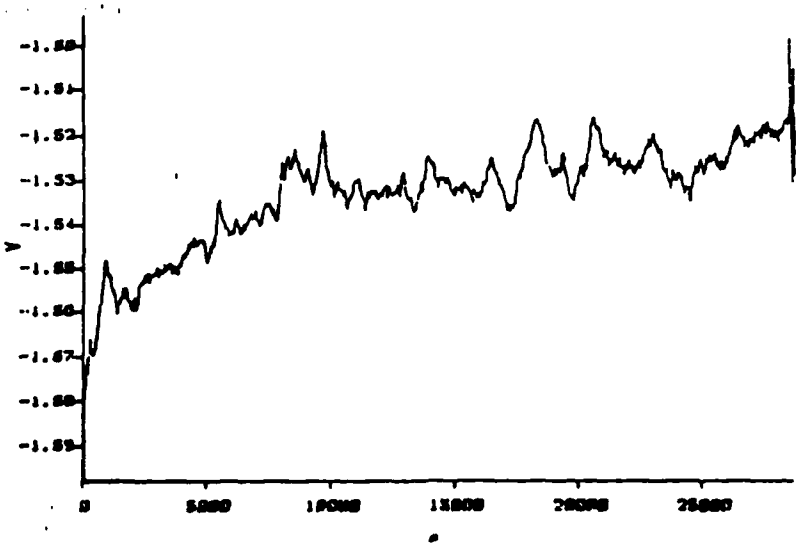

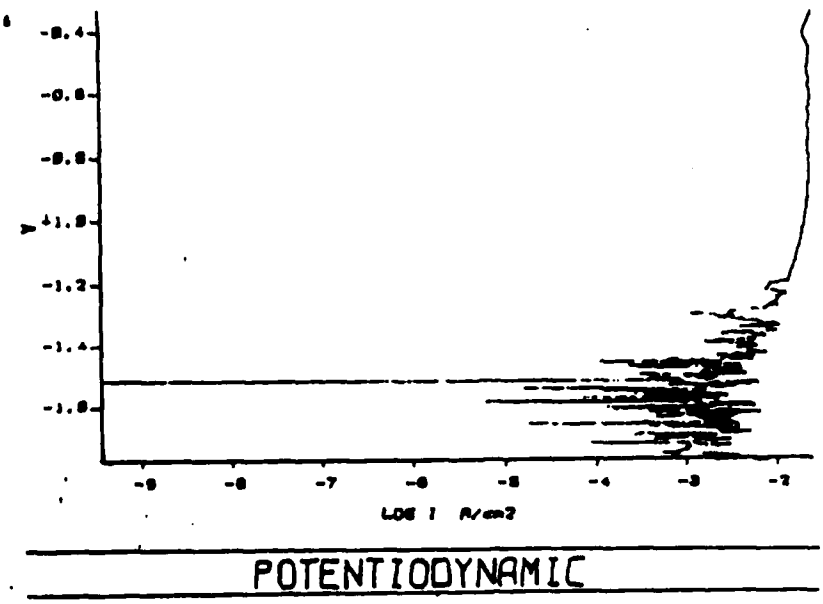

12b Potentiodynamic Plot of Pure Mg

Fig. 13a Corrosion Potential Plot of Laser Clad Region

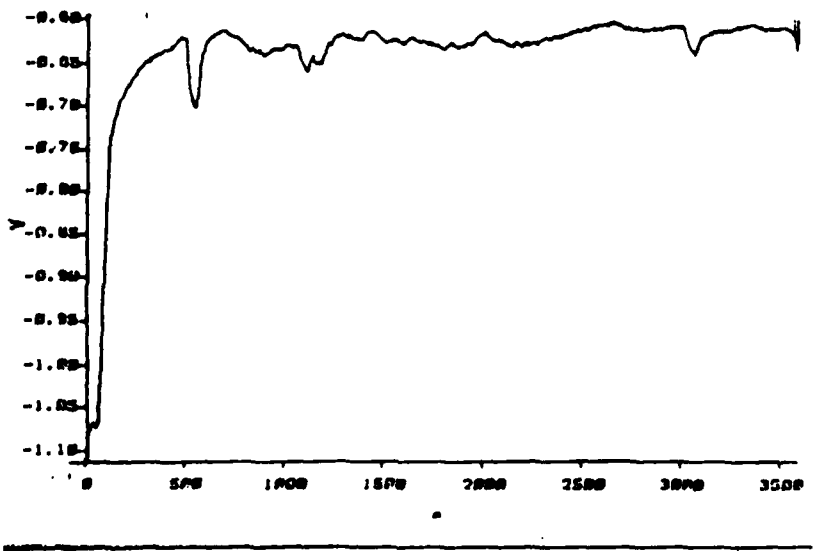

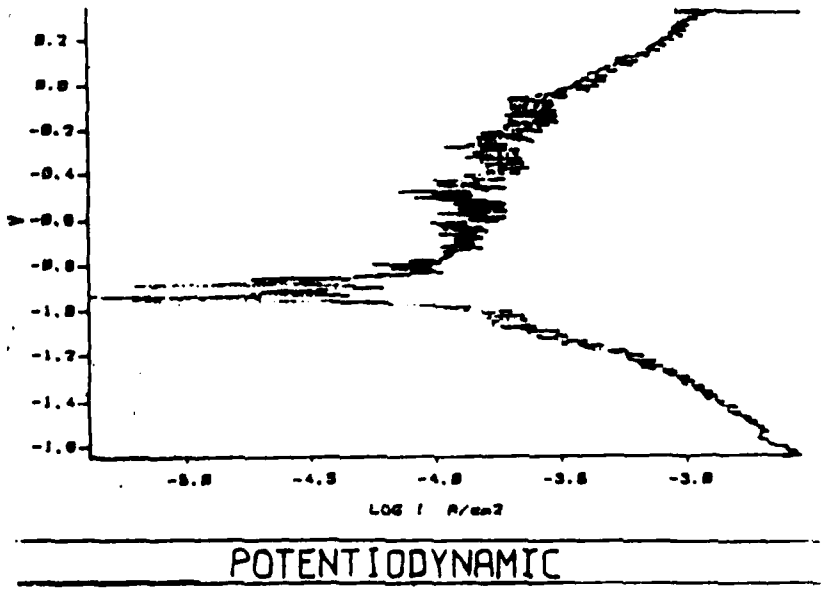

13b Potentiodynamic Plot of Laser Clad Region

Figs. 14 and 15 Optical Mircograph of Clad Region of Ti Laser Cladded onto Nb at 8 kW, 20 ipm (inches per minute)

Figs. 16 and 17 Optical Micrograph of Clad Region of Ti Laser Cladded onto Nb at 6 kW, 20 ipm

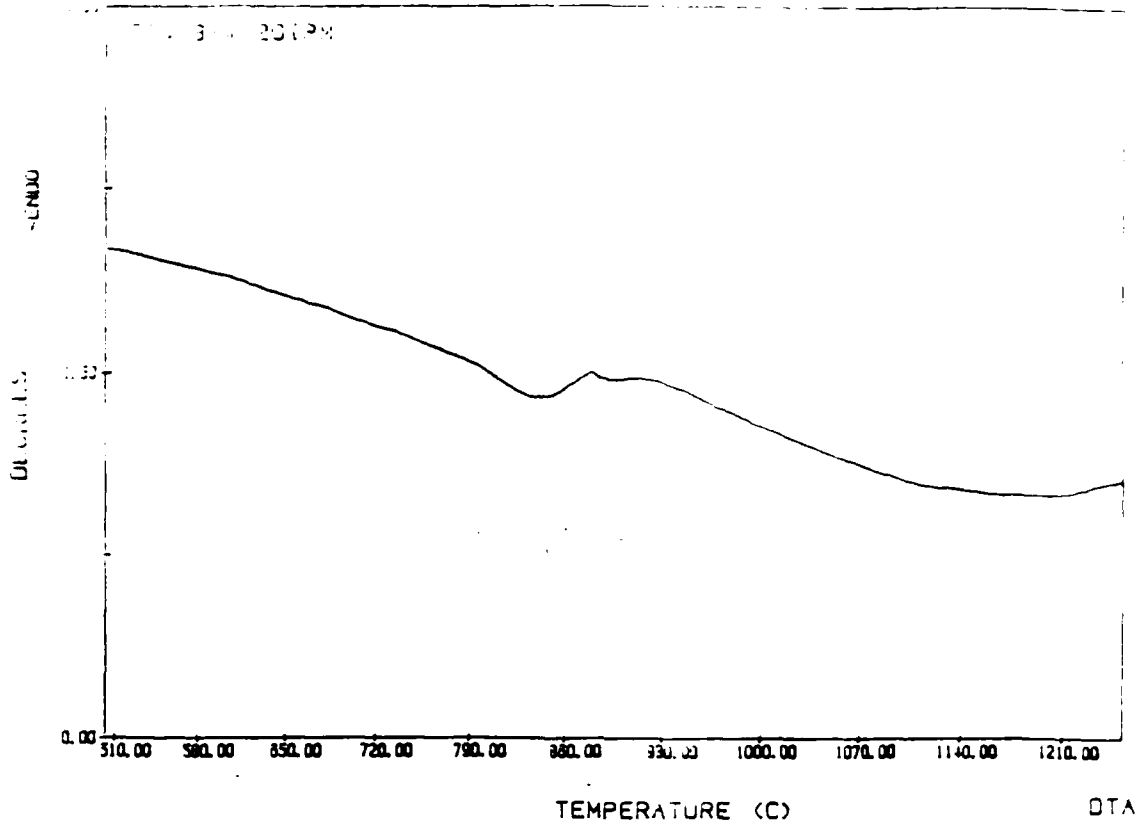

Fig. 20 DTA - Heating Curve of Ti Clad Region - 8 kW, 20 ipm

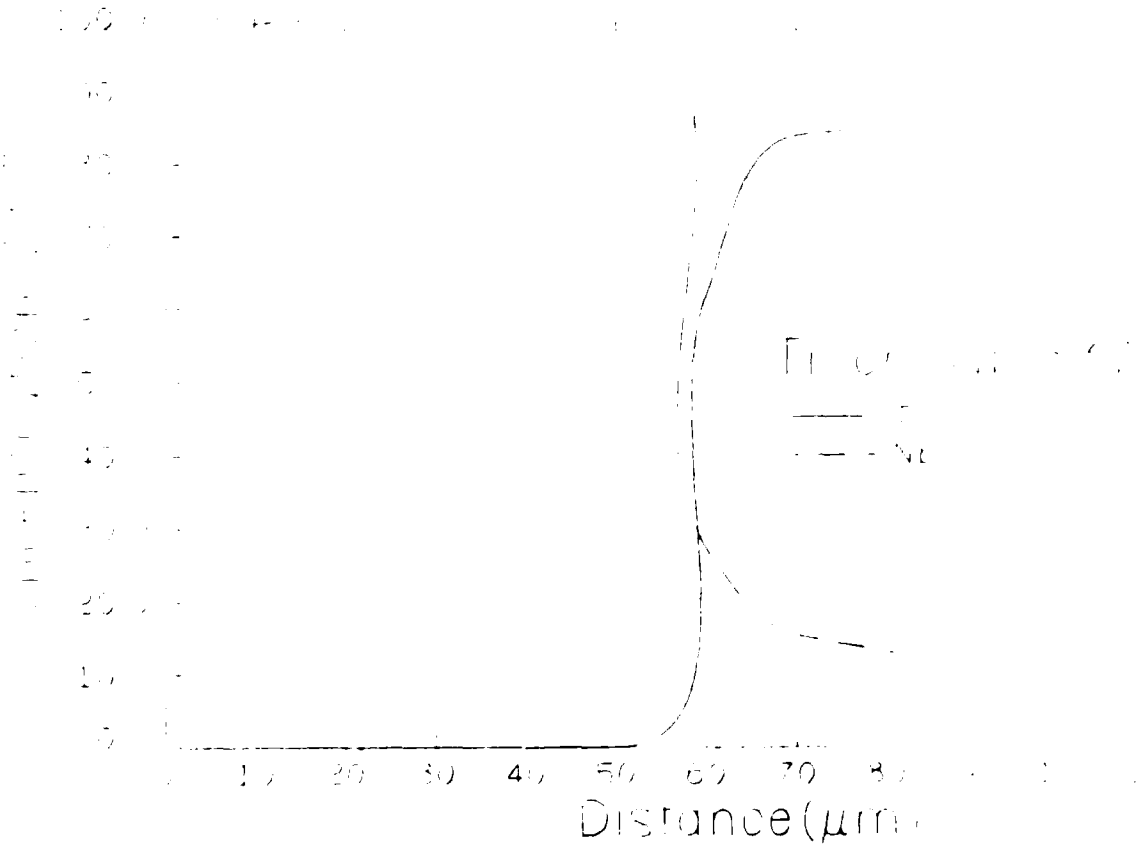

Fig. 21 EPMA - Curve of Ti/Interface/Nb - 8 kW, 20 ipm

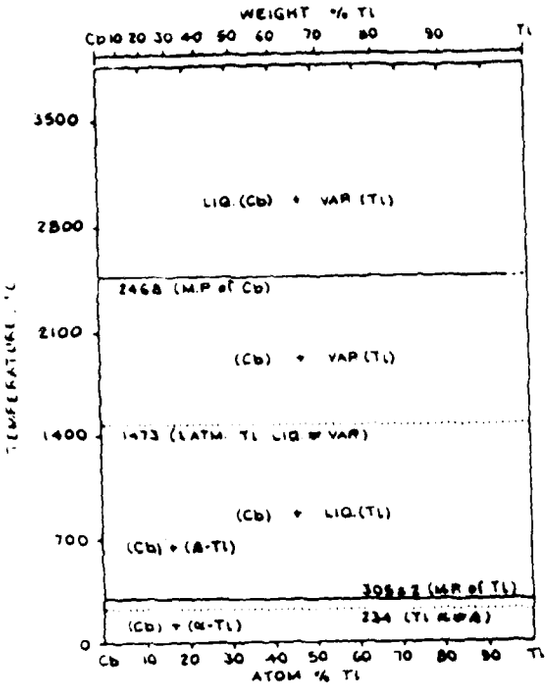

Diag am from ref. 1 except 1-atm. Ti LIQ. ⇌ VAP. and α ⇌ β transition temperatures added by Handbook compiler. No intermedia phases were found, even after holding for two months at 500°C and 7 kbar pressure. The system exhibits mutual insolubility of the component elements.

(1) Villars, P. and Girgis, K.
"Die Zustandbilder Nb-In, Nb-Tl, Ta-In und Ta-Tl."
Z. METALLKUNDE; 73 (1982); Pp 169-171

11/82

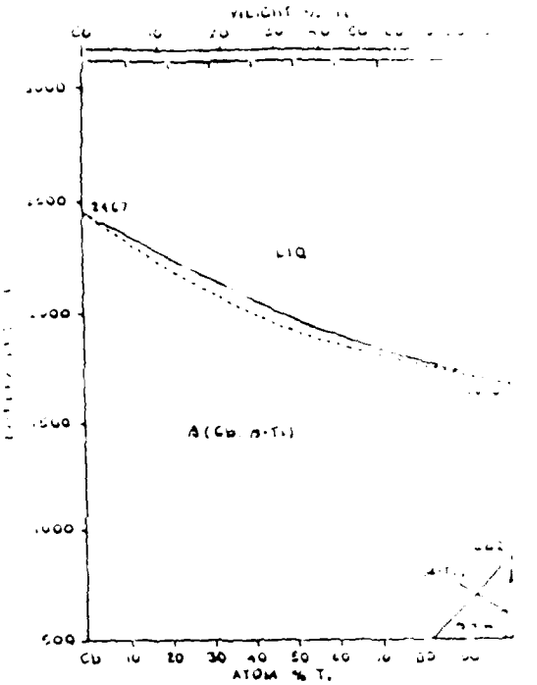

redrawn from system evaluation of ref. ... crystallography through 1978. This diagram is not different ... ure from that of Hansen Fig. 560 which, however, ... considerably greater spread between liquidus and solidus ... ref. 1 for information on crystal structures, thermod... ...d metastable phases.

(1) Murray, J.L.
"The Nb-Ti (Niobium-Titanium) System."
BULL. ALLOY PHASE DIAGRAMS; 2(1), 1981 ...

Fig. 22 Equilibrium Phase Diagram of Nb-Ti

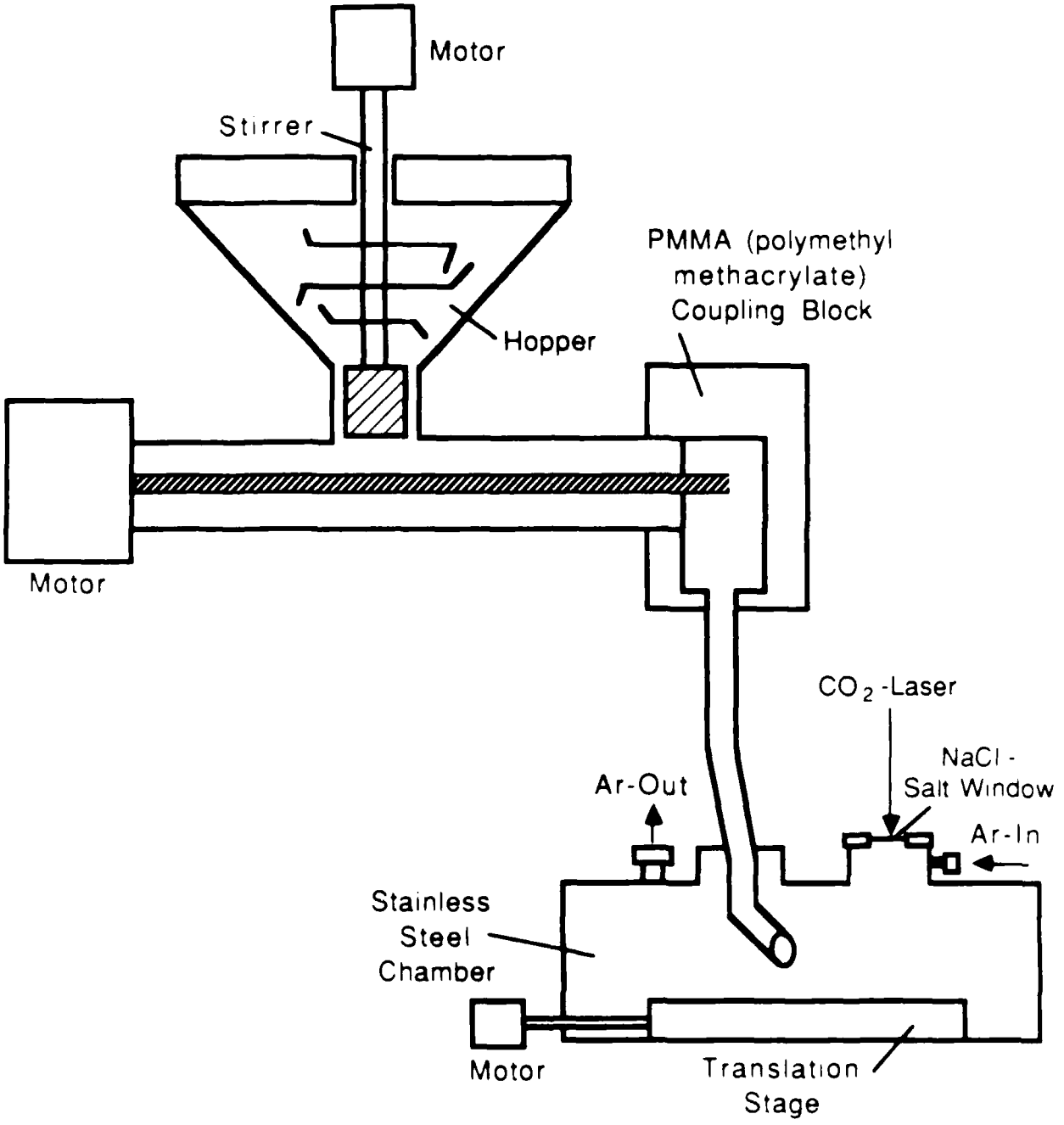

Fig. 23 The Schematic Diagram of Screw Feeder Developed to Carry Out In Situ Laser Cladding

Table 1 Composition of Amorphous and Crystalline Regions of Fig. 5

Region	Composition in weight % Mg	Zr
A-amorphous	15.367	84.634
B-interface	49.431	50.569
C-crystalline	74.464	25.536

Table 2 Corrosion Evaluation of Zr Laser Cladded onto Mg and Comparison with other Alloy Systems

Corrosion Evaluation:	3.5%-NaCl
Material:	E-Corrosion
Zr-Laser Clad	-0.647
Al-Cold Rolled	-0.674
Al-Powder Compact	-0.733
Al-Laser Clad	-1.335
Mg-As Received	-1.526
Mg-Alloy	-1.455

Table 3 High Temperature Strength of Nb Alloys UTS (MNm^{-2})

Alloy	1,100°C	1,320°C	1,540°C	1,760°C
Superalloys	245/350	---	---	---
Niobium alloys	350	168	119	---
Molybdenum alloys	630	385	252	182
Tantalum alloys	560	364	210	105
Tungsten alloys	700	420	280	210
Chromium alloys	315	119	---	---

Table 4 Laser Cladding Process Parameters

Ti Cladded onto Nb

Power	Beam Diameter	Scanning Speed
4 kW	3 mm	20 ipm
6 kW	3 mm	50 ipm
6 kW	3 mm	20 ipm
8 kW	3 mm	20 ipm

REFERENCES

1. Mukherjee, K., and J. Mazumder, "Laser Processing of Materials," Conference Proceedings, TMS, AIME, 1985.

2. Weinman, L. S., Devault, J. N., Moore, P., "Applications of Lasers in Materials Processing," American Society for Metals, Metals Park, OH, pp. 245-257, April 1979.

3. Molian, P. A., Scr. Metall. Vol. 17, No. 11, pp. 1311-1314, 1983.

4. Walker, A., West, D. F. F., Steen, W. M., Met. Technol., Vol. 11, No. 9, pp. 399-404, 1984.

5. Weerasinghe, V. M., Steen W. M., "Transport Phenomena in Materials Processing," American Society of Mechanical Engineers, pp. 15-23, 1983.

6. Inoue, A., Iwadochi, T., Minemura, T., and Masumato, T., Trans. J. I. M., Vol. 22, p. 197, 1981.

7. Messler, R. W., Ansell, G. S., and Lizunov, V. I., Trans. ASME, Vol. 62, p. 213, 1981.

8. Molian, P. A., Wang, P. J., Khan, K. H., and Wood, W. E., in the Material Research Society Proceedings of "Rapidly Solidified Amorphous and Crystalline Alloys," ed. B. H. Rear, B. C. Griessen, M. Cohen, North Holland Publishing Company, Vol. 8, p. 511, 1981.

9. Rayment, J. J., and Thomas, G., ibid, p. 547.

10. Kattamis, T. Z., "Solidification Microstructure of Laser Processed Alloys and its Impact on Some Properties," Lasers in Metallurgy, Met. Soc. AIME, pp. 1-10, 1981.

11. Kalimullin, R. K. H., Kuzhevnikov, Y. Y., "Structure and Corrosion Resistance of Nb-Li Base Alloy after Laser Treatment," Mat. Sci. Neat Treat (USSR), Vol. 27, No. 3/4, pp. 272-274, 1985.

12. Lyutyi, E. M., Gomozov, L. I., Eliseena, O. I., Fi. Khim. Mekh. Mater., Vol. 2, pp. 122-124, 1985.

13. Domashevskaya, E. P., Metallorzika, Vol. 17, No. 37, pp. 31-36, 1985.

14. Korotaev, et al., Fiz, A.D., Met. Metalloved, Vol. 54, p. 6, 1982.

15. Troitskii, B. S., Zakharov, A. M., Vergasova, L. C., Vlasov, P. N., Izr, V. U. Z. Tsvetn. Metall., Vol. 6, pp. 71-74, 1981.

16. Draper, et al., C. W., "Laser and Electrons Beam Interactions with Solids," Elsevier Science Publications, pp. 419-424, 1981.

17. Goward, G. W., "Overview Protective Coatings--Purpose, Role and Design," MTS, Vol. 2, No. 3, pp. 194-200, 1986.

18. Bill, R., Appleton, Bruce Sartwell, Paul, S. Peercy, Robert Schaefer, and Richard Osgood, Materials Science and Engineering, Vol. 20, p. 23, 1985.

19. Domashevskaya, E. P., Metallofizika, Vol. 7, No. 3, pp. 31-36, 1985.

20. Christian Perrin, Titanium 80 Science and Technology, Proc., 4th International Conference on Ti, Vol. 4.

21. Oshima, M., et al., Solid State Communication, Vol. 46, No. 11, pp. 815-818, 1983.

22. Maksimovich, et al., Fiz. Khim, Mekh. Meter. Vol. 4, pp. 82-86, 1984.

23. Korotaev, et al., AD., Fiz. Met. Metalloved., Vol. 54, No. 6, 1982.

24. Troitskii, et al., B. S., Izv. V. U. Z. Tsvetn. Metall., Vol. 6, pp. 71-74, 1981.

25. Lyutyi, et al., E. M., Fiz. Khim. Mekh. Mater., Vol. 2, pp. 122-124, 1985.

26. Kozlov, et al., A. T., IZV. Akad. Naul, SSSR, Met. Vol. 3, pp. 182-186, 1985.

27. Belov, et al., A. F., Izv. Akad. Nauk, SSSR, Met., Vol. 5, pp. 92-97, 1982.

28. Troitskii, et al., BS., Sov. Nonferrous Met. Res., Vol. 9, No. 6, pp. 500-503, 1981.

29. Voitovich, et al., RV., Russ. Met., Vol. 1, pp. 183-187, 1979.

30. Fedotov, Ak., IZV. Akad, Nauk. SSSR, Met., Vol. 5, pp. 248-252, 1979.

31. Shatinskii, et al., VF., Prot. Met. (USSST), Vol. 15, No. 3, pp. 301-303, 1979.

32. Vasileva, et al., E. V., Tr Moskov Vyshh Etkh Univ NE Bauman, Vol. 214, pp. 63-67, 1976.

33. Critical Materials in the Electrical and Electronics Industry. The Inst. of Metallurgists, pp. 35.

34. Kofstad, P., et al., Technical Scientific Note, Vol. 3, 1960.

35. Argent, B. B., et al., J. Less-Common Metals, Vol. 2, Nos. 2-4, p. 181, 1960.

36. Felten, E. J., J. Less Common Metals, Vol. 17, p. 207, 1969.

37. Smith, R., J. Less-Common Metals, Vol. 2, 1960.

38. Pfeiffer, I., Hack, S., Z. Metallkd., Vol. 72, No. 1, pp. 36-42, 1981.

39. Capelli, P. G., "Laser Surface Alloying," Agard, Naho, (LS-106), pp. 13, March 1980.

END

5-81

DTIC